Numerical Study on the Use of a Sinusoidal Leading Edge for Passive Stall Control at Low Reynolds Number

J. F. D. Câmara[1]

Detached eddy simulations have been performed for both infinite and finite wings using a sinusoidal leading edge for passive stall control at a Reynolds number of 160,000. The global effect of this geometrical modification was initially assessed in terms of aerodynamic characteristics, namely lift and drag. Detailed analyses of the flow topology have been obtained through the visualization of instantaneous vortical structures. The numerical simulations have demonstrated the ability of catching the bi-periodic flow pattern reported in published experiments for infinite wings. Simulations carried out for a unity aspect ratio finite wing have also been validated against experimental aerodynamic data. Finally, an explanation for the nature of the streamwise vortical structures emanating from the sinusoidal leading edge has been proposed.

Nomenclature

AR	=	aspect ratio
C_p	=	pressure coefficient
C_L	=	lift coefficient
C_D	=	drag coefficient
c	=	wing chord, m
Re	=	Reynolds number

I. Introduction

THE interest in micro air vehicles (MAVs) has increased in the last decades, accompanied by the technological advance demanded for their development. Such vehicles can nowadays perform a wide number of tasks, fulfilling

[1] A similar version of this paper, made in co-authorship with Prof. J.M.M. Sousa, has been accepted for oral presentation in the 51st AIAA Aerospace Sciences Meeting to be held on 7-10 January 2013 in Grapevine, Texas, United States of America.

intelligence, reconnaissance, target acquisition and designation functions, possibly replacing humans in harsh, hostile environments. However, due to the small size and low velocities of MAVs, they operate in the low Reynolds number regime ($Re < 200{,}000$), which, compared to the high Reynolds number range, has not its aerodynamics well established yet. Hence, conventional (i.e. high *Re*) aerodynamic solutions may not work as expected [1]. Laminar separation and early aerodynamic stall plague the flight in the low-Reynolds-number regime, thus motivating an inescapable need for passive or active flow management.

It has been claimed that many lessons can be learned from nature and biomimetics may indeed hold the key to breakthrough improvements in a variety of fields, namely in aerodynamics. For example, observations of the hunting techniques of humpback whales (Megaptera novaeangliae) have shown that they are able of performing acrobatic maneuvers and tight curves [2]. It was subsequently suggested that the scalloped leading edge of their pectoral flippers was somehow improving their hydrodynamic performance [3]. Further studies have confirmed that the use of this idea for the modification of the leading edge to a sinusoidal shape allowed to prevent the abrupt fall in lift at stall, thus presenting a more gradual decrease of lift instead [4-7]. Other studies report that such modification was able to delay the occurrence of stall as well [8]. The resulting aerodynamic behavior was suggested to be caused by the vortices created by the sinusoidal leading edge, which, acting as wing fences, prevent spanwise motions and the spread of separated flow regions [6, 9-10]. In addition, the energizing influence of these streamwise vortices in the aft portion of the wing [3, 6, 9] makes it a promising solution for passive stall control at low Reynolds numbers.

The majority of the studies on this subject published to date consist in experimental investigations of infinite wing configurations operating at moderate Reynolds numbers. Only very few studies have analyzed the application of this bio-inspired technique to finite wings operating at low Reynolds numbers. However, before embarking in detailed analyses of low-aspect-ratio wings, it is important to understand better the flow mechanisms associated to the vortical structures generated by the sinusoidal leading edge in the absence of wing tip effects. The currently accepted explanation is that the formation of the streamwise vortices takes place in the protuberances, analogously to those of a delta-wing [5]. In the present paper we propose the use of detached eddy simulations (DES) to firstly investigate an infinite wing configuration. It will be shown that the DES was able to catch a number of features experimentally documented in previous work. Secondly, and envisaging a future application to MAVs, the extension to a finite wing configuration is presented and validated against recent experimental data. We finalize by suggesting an alternative description for the mechanism of formation of the streamwise vortices.

II. Numerical Methodology

A. Wing Models

The models were originally constructed using the CAD software Solidworks, based on a prescribed wing section. The airfoil NASA LS(1)-0417 was chosen for this purpose because it is characterized by a large leading edge radius, thus resulting in a more predictable stall [11]. Moreover, despite the fact that the use of thick airfoils is discouraged at low Reynolds numbers, the larger space available for payload in the enclosed volume may present an advantage over the usual thin profiles for MAV applications [7]. In order to generate the sinusoidal leading edge, the reference wing section had to be modified without distorting the trailing region. It was decided that the original airfoil should correspond to zero amplitude points in the sinus wave. Hence, the profiles located at smaller chord zones than the reference (*valleys*) have larger leading edge radii and the profiles corresponding to maximum amplitude zones, displaying larger chords (*peaks*), are relatively thinner than the reference geometry and have a smaller leading edge radius. The mean chord of all the models used in the present study was kept constant. The amplitude and the wavelength of the sinus wave were fixed to 0.12*c* and 0.5*c*, respectively [6, 7]. Table 1 summarizes the variations considered for infinite wing simulations, corresponding model B to the clean (baseline) geometry and models S1 to S3 to sinusoidal geometries with different numerical aspect ratios and distinct locations of the *peak*/*valley* zones. Model S3 was later used for finite wing simulations as well, using square wing tips. As a result, the wing ends abruptly but this option has the advantage of avoiding the addition of extra variables to the design of the models.

Table 1 Specifications of the models used in infinite wing simulations

Model	Numerical *AR*	Centerline	Sinus amplitude	Sinus wavelength
B	0.25	–	–	–
S1	0.5	*peak*	0.12*c*	0.5*c*
S2	1	*peak*	0.12*c*	0.5*c*
S3	1	*valley*	0.12*c*	0.5*c*

B. Computational Meshes

A C-topology was selected to generate the computational meshes around the models used in infinite wing simulations. The farfield boundary was set at a distance of 20*c* in all non-spanwise directions. In these simulations a periodicity condition was imposed at the spanwise face boundaries of the computational domain. No-slip conditions were applied along the wall surfaces of the wing. Aiming to properly resolve the wall boundary layers, mesh nodes

were clustered near wing surfaces using a geometric expansion. Finally, as the flow remained incompressible in all studied cases, a simple open boundary condition was used at the outflow section. Depending on the model specified in Table 1, the total number of mesh nodes varied from about 2 million (model B) to 8 million (models S2 and S3).

The computational mesh for finite wing simulations was generated around the S3 model employing a C-H-topology instead. In this case, the periodic boundaries were replaced by additional farfield boundaries. A geometric expansion was again used, now along the spanwise direction also, in order to cluster mesh nodes in the vicinity of the wing tips. As a consequence of the augmented size of the computational domain, the total number of mesh nodes had to be increased to about 10 million.

C. Numerical Simulations

Taking into account the geometry of the models and the selected Reynolds number, LES (Detached Eddy Simulation) and DNS (Direct Numerical Simulation) were deemed too computationally expensive and, therefore, were discarded. We chose DES (Detached Eddy Simulation) over unsteady RANS (Reynolds Averaged Navier-Stokes) as DES is known to perform better when massive separations occur [12], which is expected to arise for the models operating at high angles of attack. DES is a hybrid between LES and RANS, as it uses the latter to resolve the boundary layer. For this purpose, the selected turbulence model was the SST k-ω [13]. The reason is twofold: firstly, because this modeling procedure can be coupled with transition prediction via a transport equation for intermittency; secondly, because of the superior performance of this model at reducing the mesh influence of the DES limiter in the RANS boundary layer [12].

The numerical procedure used a SIMPLE (Semi-Implicit Method for Pressure Linked Equations) pressure-velocity coupling and a second-order accurate spatial discretization for the pressure. The QUICK (Quadratic Upwind Interpolation for Convective Kinematics) scheme was used in the discretization of momentum and turbulence equations [14]. However, the time integration was performed employing a second-order accurate implicit scheme to alleviate numerical stability restrictions. The time step used was 0.0025 s in all simulations. The model chord and the freestream velocity were fixed to 0.25 m and 9.35 m/s, respectively. This corresponded to a Reynolds number *Re* of 160,000, within the typical range of operation of MAVs. In a large number of cases the simulations had to be carried out for longer than 40 s in order to reach a stable (unsteady) behavior unaffected by initial transients.

III. Results and Discussion

A. Infinite Wing Simulations

The analysis of the effect of the use of the sinusoidal leading edge at low Reynolds number was initially carried out based on its impact in lift and drag coefficients, C_L and C_D, with respect to the reference geometry. Figure 1a shows the evolution of C_L for increasing values of the angle of attack for models B and S1. It can be seen that the reference wing stalls at angles of attack larger than 16 degrees. This is confirmed by the steep jump observed in C_D past that incidence value, as shown in Figure 1b. In contradistinction, model S1 does not seem to stall up to an angle of attack as high as 20 degrees. However, this modified geometry exhibits degradation in C_L at low (positive) angles of attack. The corresponding C_D values are only slightly higher than those shown by model B in this range (up to an angle of attack of approximately 7.5 degrees). However, much higher C_D values result for model S1 at higher angles of attack, indicating that the improved behavior exhibited in lift at that range is obtained at the expense of a higher drag. Figure 1b further confirms that stall was not observed for model S1. Altogether, these simulations indicate a better C_L performance at high angles of attack than that presented in previously published experiments [6]. An explanation for the discrepancy may perhaps be found on the use of a thicker wing section by those authors, as well as a slightly higher Reynolds number. On the other hand, the C_D evolutions are strikingly similar, except at low angle of attack.

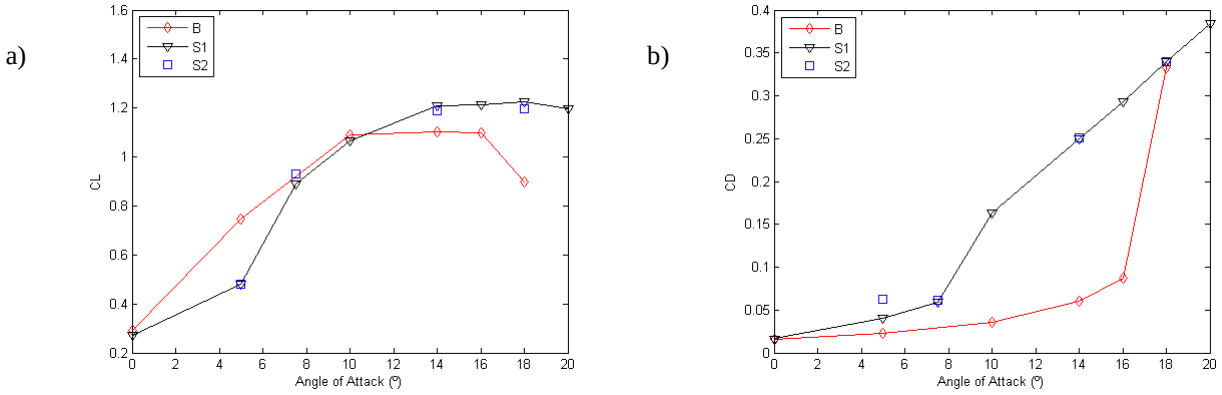

Fig. 1 Aerodynamic characteristics of reference (B) and sinusoidal models (S1 and S2): a) lift and b) drag.

Results of the simulations carried out for model S2 were also included (symbols only) for selected angles of attack. The use of a larger numerical aspect ratio in the simulations seemed to produce only a negligible effect on the

calculated values of C_L and C_D. However, model S2 was required in order to be able of reproducing the bi-periodic flow pattern reported in infinite wing experiments at moderate to high angles of attack [6]. Figures 2a and 2b shows instantaneous flow fields obtained at an angle of attack of 7.5 degrees for models S1 and S2, respectively. Similar representations are provided in Figs. 3a and 3b for an angle of attack of 18 degrees. The flow fields are illustrated in terms of vorticity surfaces ($\Omega = 20$) and pressure coefficient contours ($-2.5 < C_p < 0.2$). It must be noted that only the basic topology should be compared as distinct time instants have been plotted. Taking this into consideration, it can be seen that the streamwise vertical structures formed at the *valley(s)* of the leading edge remain approximately periodic along the spanwise direction at the lower angle of attack. However this is not the case anymore at the higher incidence, although such phenomenon can only be observed when model S2 is used. A direct comparison between the bi-periodic pattern obtained here and that visualized in water tunnel experiments [5] is portrayed in Fig. 4.

a) b)

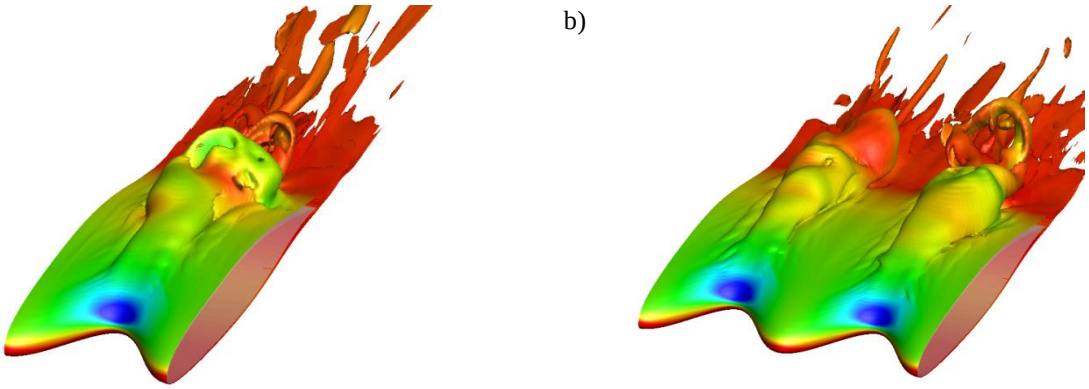

Fig. 2 Instantaneous flow fields at an angle of attack of 7.5 degrees: a) model S1 and b) model S2.

a) b)

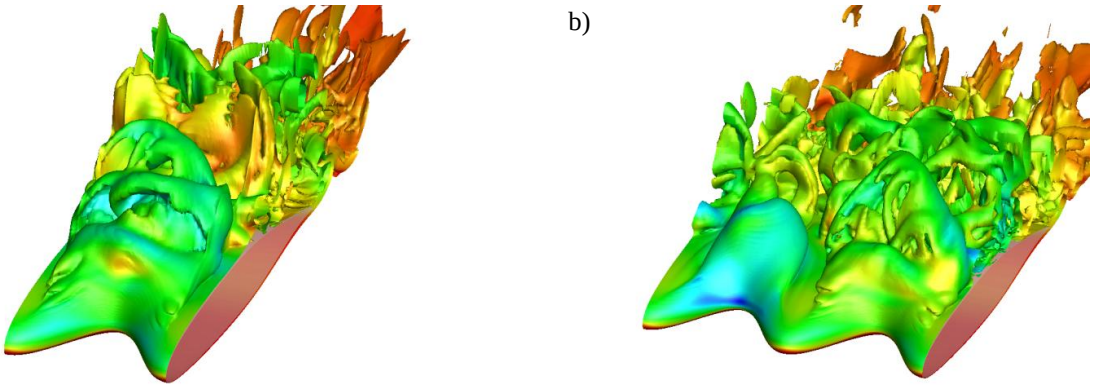

Fig. 3 Instantaneous flow fields at an angle of attack of 18 degrees: a) model S1 and b) model S2.

a) b)

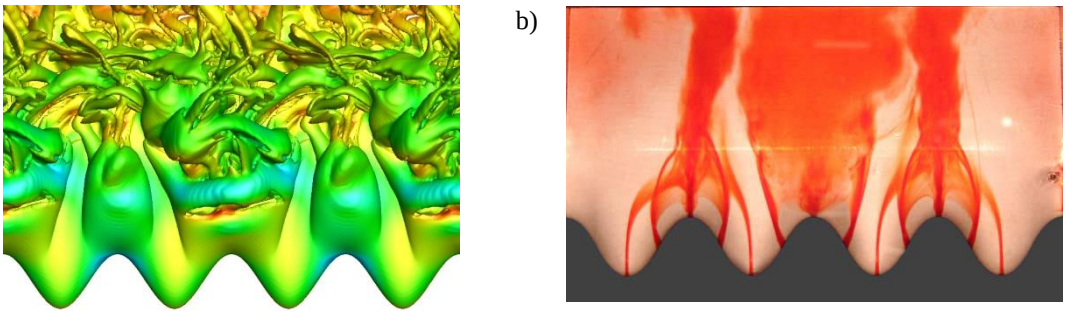

Fig. 4 Bi-periodic flow pattern visualized at an angle of attack of 14 degrees: a) simulations and b) experiments [5].

B. Finite Wing Simulations

Model S3 was considered in the previous section (results not shown) simply as an intermediate step to be taken before extending the present simulations to a low-aspect-ratio finite wing. This was required in order to ensure the reproduction of published experiments [7]. Simulations have been made at this stage for a unity aspect ratio only. In the aforementioned work it was shown that best results were obtained for an aspect ratio of 1.5. However, in the present work we have focused on the analysis of the numerical aspects of the simulations and on the physical mechanisms resulting from the use of a sinusoidal leading edge at low Reynolds number.

Figure 5 illustrates a comparison of both experimentally and numerically obtained drag polars for the finite wing. Moderate deviations were found, with consistently lower values computed for the drag coefficient, but their origin remains to be clarified.

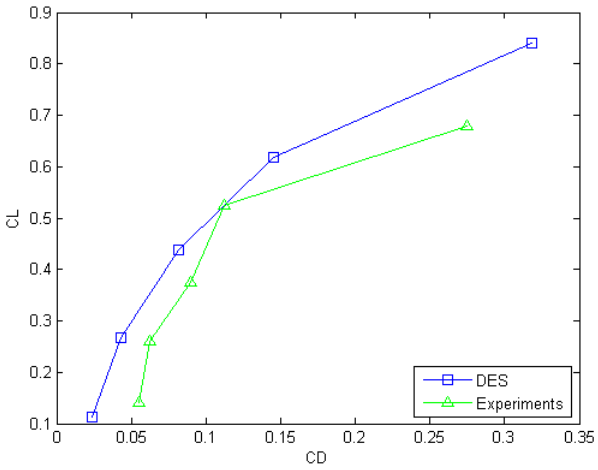

Fig. 5 Drag polar for the unity aspect ratio finite wing: simulations vs. experiments [7].

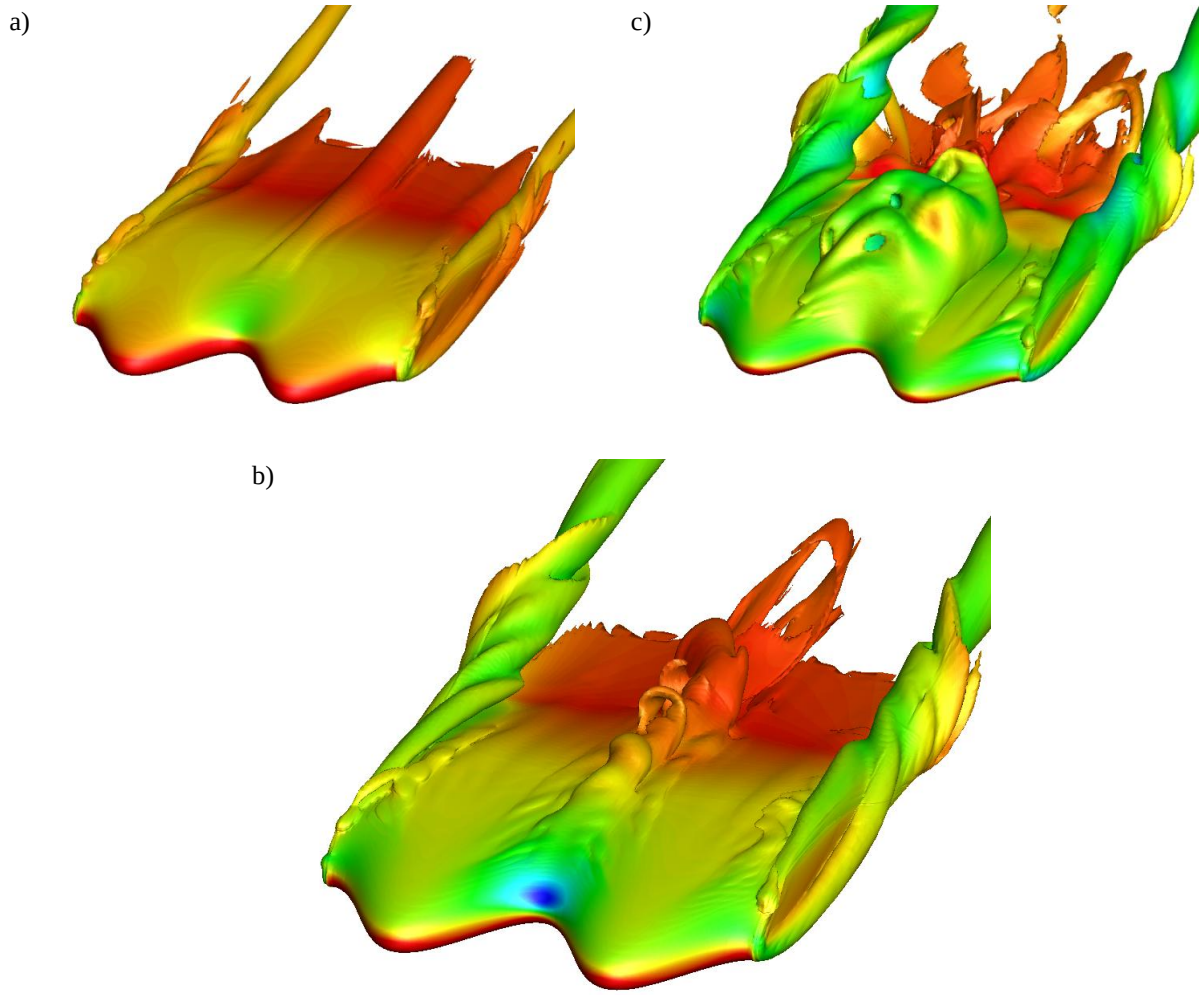

Fig. 6 Instantaneous flow fields for the finite wing of unity aspect ratio at various angles of attack: a) 5 degrees, b) 15 degrees and c) 22 degrees.

Similarly to the procedure previously followed for infinite wing simulations, instantaneous representations of the flow field have been produced for the finite wing as well. Figure 6 depicts how the basic topology of the flow changes as the angle of attack is increased. The main difference with respect to the previously discussed infinite wing simulations is the obvious appearance of the tip vortices. However, for a unity aspect ratio, these vortices allow the formation of only one of the streamwise vortical structures emanating from the *valley* at the sinusoidal leading edge. Strong unsteadiness is still observed in these structures at moderate (Fig. 6b) to high (Fig. 6c) incidences. The presence of the tip vortices also seems to enhance the organization of the flow structures in the centerline region,

which strongly resemble a train of hairpin vortices. An explanation for this is proposed as follows: the low pressure at the valley produces an upwards stream characterized by high local velocities; this stream subsequently encounters the freestream crossflow on the upper side of the wing; the local flow may be approximated to a jet in crossflow, thus yielding the widely known formation of a train of hairpin-like vortices along the main flow direction.

IV. Conclusion

The use of a sinusoidal leading edge for passive stall control at low Reynolds number has been investigated numerically with detached eddy simulations. Both infinite wing and a unity aspect ratio finite wing have been considered. The geometrical characteristics of the sinus wave were kept constant in this study, corresponding to an amplitude and wavelength of 0.12*c* and 0.5*c*, respectively.

Lift and drag characteristics of the modified geometry have been compared with those of the baseline, for an infinite wing. Delay of aerodynamic stall was achieved at the expense of a lift reduction at low incidences and a significant drag penalty at angles of attack smaller than the stall angle of the baseline. Drag polars obtained from the present simulations and previous experiments have also been compared for the finite wing. The flow topology was studied in detail through the visualization of instantaneous vortical structures. Special features of these streamwise structures have been identified and discussed with reference to published experiments.

Acknowledgments

This work was funded by Fundação para a Ciência e aTecnologia, under project PTDC/EME-MFE/122849/2010. The first author would also like to acknowledge João Guerreiro for fruitful discussions.

References

[1] Mueller, T. J., and DeLaurier, J. D., "Aerodynamics of Small Vehicles," *Annu. Rev. Fluid Mech.*, Vol. 35, Jan., 2003, pp. 89-111.
doi: 10.1146/annurev.fluid.35.101101.161102

[2] Edel, R. K., and Winn, H. E., "Observations on Underwater Locomotion and Flipper Movement of the Humpback Whale *Megaptera novaeangliae*," *Marine Biology*, Vol. 48, No. 3, 1978, pp. 279-287.
doi: 10.1007/BF00397155

[3] Fish, F. E., and Battle, J. M., "Hydrodynamic Design of the Humpback Whale Flipper," *Journal of Morphology*, Vol. 225, No. 1, 1995, pp. 51-60.

doi: 10.1002/jmor.1052250105

[4] Hansen, K. L., Kelso, R. M., and Dally, B. B., "An Investigation of Three-Dimensional Effects on the Performance of Tubercles at Low Reynolds Number," *17th Australasian Fluid Mechanics Conference Proceedings*, 5-9 December 2010, The University of Auckland, Auckland.

[5] Custodio, D. S., "The Effect of Humpback Whale-like Leading Edge Protuberances on Hydrofoil Performance," M.Sc. Thesis, Dpt. of Mechanical Engineering, Worcester Polytechnic Institute, Worcester, MA, 2007.

[6] Johari, H., Henoch, C., Custodio, D., and Levshin, A., "Effects of Leading-Edge Protuberances on Airfoil Performance," *AIAA Journal*, Vol. 45, No. 11, 2007, pp. 2634-2641.
doi: 10.2514/1.28497

[7] Guerreiro, J. L. E., and Sousa, J. M. M., "Low-Reynolds-Number Effects in Passive Stall Control Using Sinusoidal Leading Edges," *AIAA Journal*, Vol. 50, No. 2, 2012, pp. 461-469.
doi: 10.2514/1.J051235

[8] Miklosovic, D. S., Murray, M. M., Howle, L. E., and Fish, F. E., "Leading-edge Tubercles Delay Stall on Humpback Whale (*Megaptera novaeangliae*) Flippers," *Physics of Fluids*, Vol. 16, No. 5, 2004, pp. 39-42.
doi: 10.1063/1.1688341

[9] Pedro, H. T. C., and Kobayashi, M. H., "Numerical Study of Stall Delay on Humpback Whale Flippers," *46th AIAA Aerospace Sciences Meeting and Exhibit*, AIAA Paper 2008-0584, Jan. 2008.

[10] Watts, P., and Fish, F. E., "The Influence of Passive, Leading Edge Tubercles on Wing Performance," *Proceedings of the Twelfth International Symposium on Unmanned Untethered Submersible Technology*, Autonomous Undersea Systems Institute, Durham, New Hampshire, 2001.

[11] McGhee, R. J., and Beasley, W. D., "Low-speed Aerodynamics Characteristics of a 17-Percent-Thick Airfoil Section Designed for General Aviation Applications," NASA TN D-7428, 1973.

[12] Bunge, U., Mockett, C., and Thiele, F., "Guidelines For Implementing Detached-Eddy Simulation Using Different Models," *Aerospace Science and Technology*, Vol. 11, No. 5, 2007, pp. 376-385.
doi: 10.1016/j.ast.2007.02.001

[13] Menter, F. R., Kuntz, M., and Langtry, R., "Ten Years of Industrial Experience with the SST Turbulence Model," *Turbulence, Heat and Mass Transfer 4*, edited by Hanjalić, K., Nagano, Y., and Tummers, M., Begell House, Inc., New York, Wallingford (UK), 2003, pp. 625-632.

[14] Pereira, J. C. F., and Sousa, J. M. M., "Finite Volume Calculations of Self-Sustained Oscillations in a Grooved Channel," *Journal of Computational Physics*, Vol. 106, No. 1, 1993, pp. 19-29.
doi: 10.1006/jcph.1993.1087